

## Article

# Effect of Ultrafine Additives on the Morphology of Cement Hydration Products

Grigory Yakovlev <sup>1</sup>, Rostislav Drochytka <sup>2</sup>, Gintautas Skripkiūnas <sup>3,\*</sup>, Larisa Urkhanova <sup>4</sup>, Irina Polyanskikh <sup>1</sup>, Igor Pudov <sup>1</sup>, Ekaterina Karpova <sup>3</sup>, Zarina Saidova <sup>1</sup> and Ali E. M. M. Elrefai <sup>5</sup>

<sup>1</sup> Department of Construction Materials, Mechanization and Geotechnics, Kalashnikov Izhevsk State Technical University, Studencheskaya Str. 7, 426069 Izhevsk, Russia; gyakov@istu.ru (G.Y.); irina\_maeva@mail.ru (I.P.); PudovIA@yandex.ru (I.P.); zarinasaيدova@mail.ru (Z.S.)

<sup>2</sup> Department of Technology of Building Materials and Components, Faculty of Civil Engineering, Brno University of Technology, Veveří 331/95, 602 00 Brno, Czech Republic; drochytka.r@fce.vutbr.cz

<sup>3</sup> Laboratory of Concrete Technologies, Faculty of Civil Engineering, Institute of Building Materials, Vilnius Gediminas Technical University, Saulėtekio al. 11, LT-10223 Vilnius, Lithuania; ekaterina.karpova@vilniustech.lt

<sup>4</sup> Department of Building Materials, Roads and Woodworking, East Siberia State University of Technology and Management, 40V Klyuchevskaya St., 670013 Ulan-Ude, Russia; office@esstu.ru

<sup>5</sup> Department of Construction Engineering, Faculty of Engineering, Egyptian Russian University, Cairo-Suez Road, Badr City 11829, Egypt; info@eruegypt.com

\* Correspondence: gintautas.skripkiunas@vilniustech.lt



**Citation:** Yakovlev, G.; Drochytka, R.; Skripkiūnas, G.; Urkhanova, L.; Polyanskikh, I.; Pudov, I.; Karpova, E.; Saidova, Z.; Elrefai, A.E.M.M. Effect of Ultrafine Additives on the Morphology of Cement Hydration Products. *Crystals* **2021**, *11*, 1002. <https://doi.org/10.3390/cryst11081002>

Academic Editors: Salman Siddique, Trilok Gupta, Yi Bao and Wei-Ting Lin

Received: 7 August 2021

Accepted: 18 August 2021

Published: 22 August 2021

**Publisher's Note:** MDPI stays neutral with regard to jurisdictional claims in published maps and institutional affiliations.



**Copyright:** © 2021 by the authors. Licensee MDPI, Basel, Switzerland. This article is an open access article distributed under the terms and conditions of the Creative Commons Attribution (CC BY) license (<https://creativecommons.org/licenses/by/4.0/>).

**Abstract:** The present research is focused on the investigation of the influence of ultrafine additives on the structure formation of hardened cement paste and the establishment of the mechanisms of the morphological transformations, which determine the properties of hydrated products. In the course of the research, the modification of ordinary Portland cement was performed by the suspension of multi-walled carbon nanotubes (MWCNTs), carbon black (CB) paste, and silica fume (SF). Scanning electron microscopy (SEM), energy-dispersive X-ray (EDX) microanalysis, X-ray diffraction (XRD) analysis, thermal analysis, and Fourier-transform infrared (FTIR) spectroscopy were used to study cement hydration products. The morphology of hardened cement paste depends on the chemical reactivity of additives, their geometry, and their genesis. The action mechanism of the inert carbon-based additives and pozzolanic silica fume were considered. The cement hydration products formed in the process of modification by both types of ultrafine additives are described. In the case of the modification of cement paste by inert MWCNTs and CB paste, the formation of cement hydration products on their surface without strong adhesion was observed, whereas in the case of the addition of SF separately and together with MWCNTs, the strong adhesion of additives and cement hydration products was noted.

**Keywords:** cement; ultrafine additives; carbon black; carbon nanotubes; silica fume; cement hydration products

## 1. Introduction

The identification of the mechanism of directional structuring during the Portland cement hydration process is one of the relevant problems of materials science in the field of creating multifunctional building materials. The predominant volume of composites for construction purposes is produced based on the hardening of binders of hydration, such as Portland cement. The management of the structure of such composites is advisable to carry out through direct impact on their hydration processes. The additives, which work as initializers of crystallization, can affect the hydration processes and create the conditions for the formation of a structure with predefined properties. Today, there are a significant number of papers on the structuring of the cement matrix due to the effects of ultrafine additives on the morphology of cement hydration products [1–13].

The setting of favorable conditions for effective hydration can be reached by the application of ultrafine additives with high surface activity caused by their small size. Among such additives, it is possible to mention carbon-based nanomaterials such as carbon black [14–17], isostatic graphite [18–20], graphene oxide [21,22], graphene nanoplatelets [23,24], carbon nanotubes [25–27], and carbon fibers [28,29]. The listed additives possess several unique properties, such as high surface energy, mechanical strength, and electrical conductivity. The application of such additives for the modification of composites provides an improvement in the structure of the binding matrix and, consequently, leads to the improvement of different composite properties [14–29].

Carbon black (CB) is a prospective additive for the design of concrete with self-sensing abilities. Monteiro et al. [14], Nalon et al. [15], and Dong et al. [16] established the improvement of electrical properties of cement composites with CB, whereas the mechanical properties, as well as microstructure, were not deeply investigated. The study of the mechanical properties of modified cement mortar was carried out by Yakovlev et al. [17]. Additionally, some researchers noted that the impact of CB on cement composites is comparable with the impact of carbon nanotubes, while the price of CB is lower [14,17].

Carbon nanotubes (CNTs) are among the most well-known and widely studied additives for the modification of cement composites. CNTs enable the obtainment of concrete with multifunctional properties [25–27]. However, the high price of CNTs and their contradictory results limit their application in construction practice. Moreover, the mechanism of action of CNTs in composites still requires further investigation [25].

Modification of cement composites by graphene oxide (GO) nanosheets leads to the densification of structure and improvement of mechanical properties. Such improvement can be explained by the fact that GO can affect the formation of cement hydration products, with the conversion of rod-like crystals to crystals with flower-like and polyhedral structures [21].

Despite the significant number of studies on the modification of cement composites with carbon-based nanoadditives, most of them are devoted to the properties of composites at the macro level, such as strength, density, porosity, etc., whereas the effect of nanoadditives on the microstructure of composites and their action mechanisms have not been deeply investigated [21,30]. The carbon-based additives without additional functionalization are inert to the cement hydration products. The formation of more stable forms of silicate hydrates can be explained by the local, equally distributed impact, high surface energy of additives, and changes in the gradient of charges [17,31].

In contrast to inert ultrafine additives, active mineral additives—such as silica fume (SF)—are quite important for managing the matrix of composites. The pozzolanic activity of these additives leads to their chemical interaction with the cement hydration products, which causes the densification of the cement matrix with the formation of silicate hydrates of another type. The significant enhancement of the microstructure of cement composites modified with SF in definite dosages, along with its effect on mechanical properties and performance, was observed in a number of studies [32–34].

Mainly, the formation of the structure of high-strength material is determined by the packing density of new formations [35,36]. The microstructure can be regulated by the usage of modifiers of different origins and dispersion degrees. Moreover, the joint modification by the additives of different origins and dispersion degrees can lead to synergistic effects on the structure of the hardened matrix [37–39].

The mechanism of complex management by the structural formation of materials is associated with the morphology of new formations in the hardened matrix through the usage of additives of different dispersity and origins. The application of ultrafine additives or their combination enables the improvement of the properties of the materials based on the mineral-binding matrix.

The present research includes the investigation of the morphology of cement hydration products in the process of modification with inert, carbon-based additives and pozzolanic silica fume. This study proposes the evaluation of formed cement hydration

products and the mechanism of the development of the microstructure of hardened cement paste in case of a modification of cement-based materials with additives of different origins, geometry, and dispersity. Our research aimed to identify the placement of different ultrafine additives concerning the cement hydration products after hardening. Despite the significant number of studies on the same topic, the effects of ultrafine additives and different complex additives based on them should be investigated further. Such factors as the geometry of additives, chemical activity of cement hydration products, and the type and intensity of their mixing in water and cement systems determine the further properties of cement composites, and explain the contradictory results obtained to date on the topic of modification with ultrafine additives. Moreover, the high cost of nanoadditives requires searching for reasonable ways to decrease the price of the modification. One of the possible decisions is the usage of ultrafine additives based on industrial waste products. The usage of waste products not only enables a decrease in the harmful impact on the environment, but can also work as an effective additive for concrete modification. However, firstly, the properties of cement composites with synthesized additives and additives based on waste products should be compared. The present research demonstrates the morphology of cement paste modified with synthesized additives (CNTs) and additives based on industrial waste products (CB, SF).

## 2. Materials and Methods

Ordinary Portland cement (OPC) without mineral additives (CEM I 42.5) (supplied by two different producers) was used in the research. The mineral composition of the cement is presented in Table 1, while its physical and mechanical properties are listed in Table 2.

**Table 1.** Mineral composition of cement.

Component	Amount, %
Tricalcium silicate (C <sub>3</sub> S)	59.0/57.9
Dicalcium silicate (C <sub>2</sub> S)	16.0/15.6
Tricalcium aluminate (C <sub>3</sub> A)	8.1/7.5
Tetracalciumaluminoferrite (C <sub>4</sub> AF)	12.0/11.9

**Table 2.** Physical and mechanical properties of cement.

Property	Value
Two-day compressive strength, MPa	15.8 ± 2.2/28 ± 2.0
Twenty-eight-day compressive strength, MPa	48.5 ± 3.0/55 ± 3.0
Initial setting time, min	150/180
Final setting time, min	200/225
Volume stability, mm	1.0/1.0
Water consumption, %	25.0/26.6
Specific surface, cm <sup>2</sup> /g	3400/3552

Potable water according to EN 1008 was used as mixing water for cement paste. Suspension of multi-walled carbon nanotubes (MWCNTs), carbon black (CB) past, silica fume (SF), and a complex of MWCNT suspension and SF were used as ultrafine additives for the modification of cement-based materials.

Aqueous suspension of MWCNTs (Figure 1a) was homogenized based on the pellets “Graphistrength CW 2-45” (“Arkema”, France). These pellets include not only MWCNTs synthesized via the chemical vapor deposition (CVD) method, but also carboxymethyl cellulose (CMC), which is used as a dispersing agent into suspension. MWCNTs have a diameter of 15–20 nm and a filament length in the range from 0.1 to 10 μm. The concentration of MWCNTs in the suspension was 1% in water. An MWCNT suspension with a mean size of agglomerates of about 220 nm was obtained (Figure 1b).

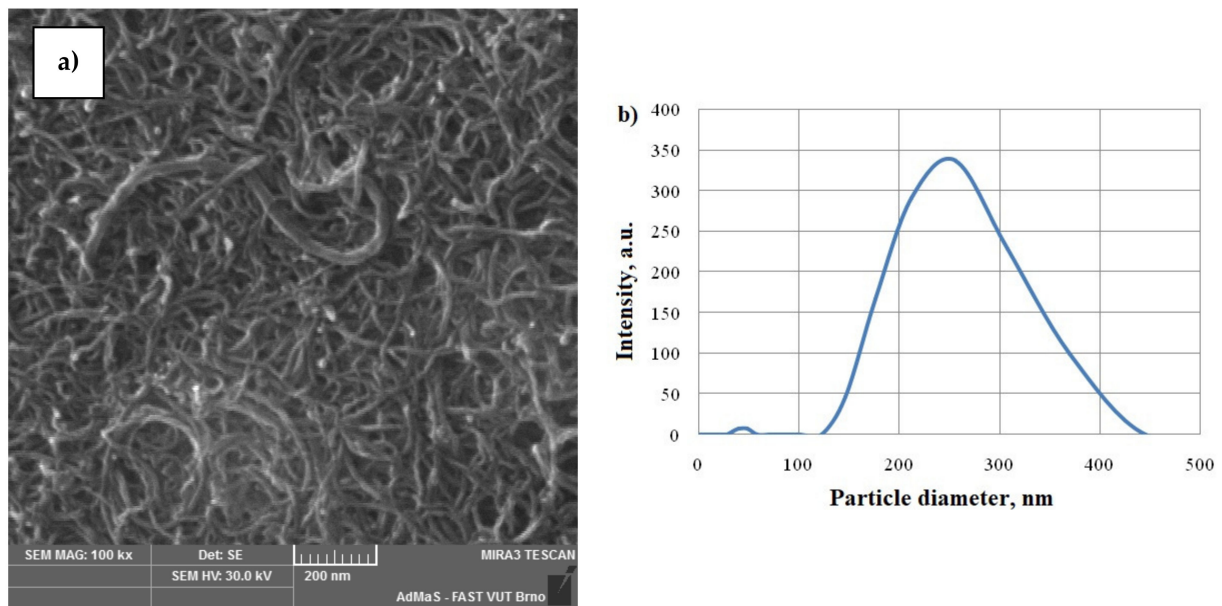


**Figure 1.** MWCNT suspension: (a) general view in an SEM image ( $\times 100,000$ ); (b) dispersion analysis.

CB is a product with specified properties, obtained as a result of the controlled pyrolysis or thermo-oxidative decomposition of liquid or gaseous hydrocarbons. According to the structure of the particles, CB takes an intermediate position between amorphous coal and crystalline graphite. The particle size of CB of  $\sim 40\text{--}110$  nm determines its high dispersity (Figure 2). In the current research, CB with a particle size up to 80 nm and a specific surface area of  $0.0065\text{--}0.0100$  m<sup>2</sup>g<sup>-1</sup> in the form of a paste was applied. The content of carbon black in the paste was 34%.

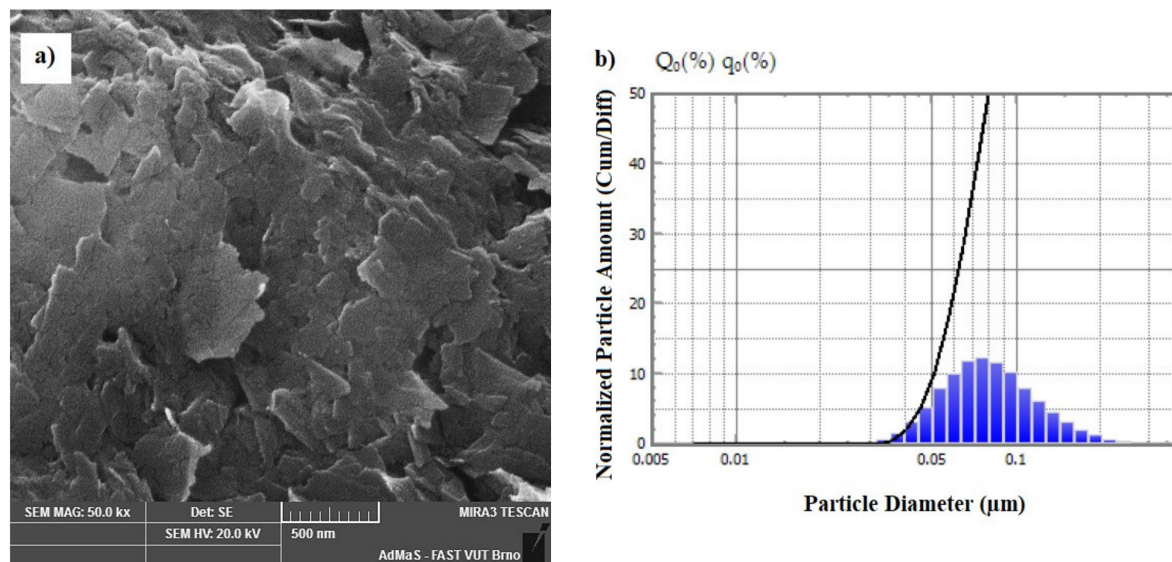


**Figure 2.** Dispersed concentrate of carbon black in an aqueous surfactant solution: (a) the microstructure of carbon black particles in an SEM image ( $\times 50,000$ ); (b) particle size distribution.

In addition to the above-mentioned additives, SF with a particle size of  $\sim 300$  nm was applied in the research. The chemical composition and physical properties of SF are shown in Tables 3 and 4, respectively.

**Table 3.** Chemical composition of silica fume.

SiO <sub>2</sub>	Al <sub>2</sub> O <sub>3</sub>	Fe <sub>2</sub> O <sub>3</sub>	CaO	MgO	Na <sub>2</sub> O	K <sub>2</sub> O	SO <sub>3</sub>	MnO
96.12%	0.86%	0.34%	0.39%	0.53%	0.21%	1.05%	0.36%	0.04%

**Table 4.** Physical properties of silica fume.

Property	Value
Color	Light grey powder
Bulk density, kg/m <sup>3</sup>	230
Specific surface, cm <sup>2</sup> /g	15–35
Pozzolanic activity, mg Ca(OH) <sub>2</sub> /g	>300
Humidity, %	<0.5
pH	5–7
Particle size dispersion, nm	14–332
Average particle diameter (more than 50% of the volume), nm	169

SF is composed of fine spherical particles with a high content of amorphous silicon dioxide, which determines its high pozzolanic activity concerning cement hydration products [34]. SF was applied together with a MWCNT suspension to investigate their complex impact on the morphology of cement hydration products. The dosages of all ultrafine additives were chosen based on the results of previous research and literature sources [17,40,41].

An ultrasonication homogenization method was used for 6 min in the preparation of the MWCNT suspension. The homogenization was performed using a Bandelin Sonopuls HD 3400 ultrasonic homogenizer (400 W, 20 kHz) with a VS 200 T probe ( $\varnothing$ : 25 mm; amplitude: 82  $\mu$ m) [40].

The CB paste was prepared using a high-speed bead mill with a speed of 10,000 rpm. Zirconium or ceramic beads are used as grinding bodies. The evaluation of the dispersity of CB paste was performed using a “SALD-7500nano” (“Shimadzu”) laser particle size analyzer (at resolution from 7 nm to 800  $\mu$ m). The dispersity of the MWCNT suspension was investigated using a “Delsa Nano C” (“Beckman Coulter”) particle size analyzer with a resolution from 0.6 nm to 7  $\mu$ m.

Scanning microscopy images of CB and MWCNT agglomerates were obtained using a Tescan MIRA 3 scanning electron microscope (SEM) with a voltage of 30 kV, at a distance from the surface of the specimen of 7–10 mm. Before SEM of the MWCNT suspension and CB paste, their thin layers were placed on the special specimen stage and dried until total drying at a temperature of  $\sim 65 \pm 2$  °C.

To study the effect of MWCNTs via SEM investigation, cement paste at a W/C ratio of 0.50 and MWCNT dosage of 0.25% by weight of cement (bwoc) were prepared. MWCNT dosage and increased content of water were applied for better observation by SEM. The MWCNT suspension was added as a part of the mixing water. The mixing of the cement paste was undertaken using a standard methodology. In the first stage, the cement pastes were observed by SEM ~1 hour after cement paste mixing at the induction period of cement hydration. Before SEM, the thin layer of cement paste was dried on the specimen stage for 30 min at a temperature of  $\sim 65 \pm 2$  °C. In the next stage, the samples with a size of 40 × 40 × 40 mm were formed and kept for 72 h in a water bath at a temperature of  $20 \pm 2$  °C.

To assess the effect of the CB on the morphology, the cement paste specimens were prepared according to the standard methodology at a W/C ratio of 0.40. CB was taken at a dosage of 0.005% bwoc. CB paste was added as part of the mixing water. The specimens before observation by SEM were kept for 28 days in a water bath at a temperature of  $20 \pm 2$  °C.

SF undergoes compaction and aggregation in conditions of natural humidity, with an increase in the mean particle size. To prevent the negative impact of aggregation, silica

fume was ground and mixed with the required amount of mixing water. The W/C ratio was set to 0.43, and the dosage of SF was 3% bwoc. The mixing procedure and preparation of specimens for SEM observation was the same as described for cement paste modified with MWCNTs and CB.

The complex modification of cement mortar with silica fume and nanotubes was carried out in the following order: The W/C ratio was set to 0.36, the SF and MWCNT dosage was 3% and 0.005% bwoc, respectively. The MWCNT suspension was added as part of the mixing water. Before addition to mixing water, SF was ground. After the introduction of all additives to the mixing water, they were mixed using a high-speed mixer at 1000 rpm for 3 min. Further addition of cement and preparation of samples was undertaken according to the standard methods. The specimens before SEM were kept for 28 days in a water bath at a temperature of  $20 \pm 2$  °C.

Before SEM, the specimens of modified hardened cement paste were dried at a temperature of  $\sim 65 \pm 2$  °C. SEM was performed on the split surface of the specimens. The distance to the surface of the specimen was between 7 and 10 mm. SEM analysis was carried using a Tescan MIRA 3 with the parameters described above. The observation of cement paste samples with silica fume and MWCNTs was explored using a JEOL JSM-7600F scanning electron microscope (SEM). The parameters of electron microscopy were as follows: voltage of 10 kV; distance from the surface of the specimen of 7–10 mm.

To reveal the phases formed in the course of modification by the different types of ultra-fine additives, X-ray diffraction (XRD) analysis and energy-dispersive X-ray spectroscopy analysis (EDX) were applied. XRD analysis was carried out using a DRON-7 diffractometer. To obtain the X-ray radiation Cu-K $\alpha$  spectrum ( $\lambda = 0.1541837$  nm), a graphite monochromator was used. The parameters of the tests were as follows: voltage of 30 kV; current of 12 mA; range of the diffraction angle of 4–80°; detector movement step of 0.02°; and duration of the intensity measuring in a step of 0.5 s. The identification of the peaks was performed using High Score XRD Analysis software with a PDF-2 powder diffraction files database. EDX was implemented via the EDX detector of the Tescan MIRA 3.

Thermal analysis of the studied hardened cement pastes was executed by using a Mettler Toledo TGA/DSC-1 (at a heating rate of 30 °C/min; the temperature varied from 50 to 1100 °C in the air atmosphere; the mass of the sample was 100 mg) and a Linseis STA PT-1000 (at a heating rate of 10 °C/min; the temperature varied from 30 to 1000 °C in the nitrogen atmosphere; the mass of the sample was 15 mg). Thermal analysis was performed on samples at an age of 28 days.

Fourier-transform infrared (FTIR) spectroscopy of the studied samples was performed at the age of 28 days using SPECTRUM GX 2000 and IRAffinity-1 spectrophotometers in a spectral range from 400 to 4000  $\text{cm}^{-1}$ . Before FTIR spectroscopy, samples were dried at  $65 \pm 2$  °C, ground, and a small number of samples (up to 2 mg) were mixed with KBr, with further pressing and formation of the probe for spectroscopy.

### 3. Results

#### 3.1. Multi-Walled Carbon Nanotubes

The addition of MWCNTs to cement paste leads to the formation of cement hydration products around the MWCNTs' surfaces (Figure 3). The SEM image of the nanomodified cement paste at the induction period of hydration shows the formation of cement hydration products, which can include calcium hydrosilicates, hydroaluminates, hydroferrites, calcium hydroxide, calcite, etc. Moreover, the observed cement paste includes a visible surface of filaments of nanotubes with straight and curved shapes. The SEM image presents the nanotubes with a diameter of  $\sim 0.1$  nm and a length more than 500 nm. Figure 4 shows that part of the MWCNTs' surfaces are covered by the cement hydration products.

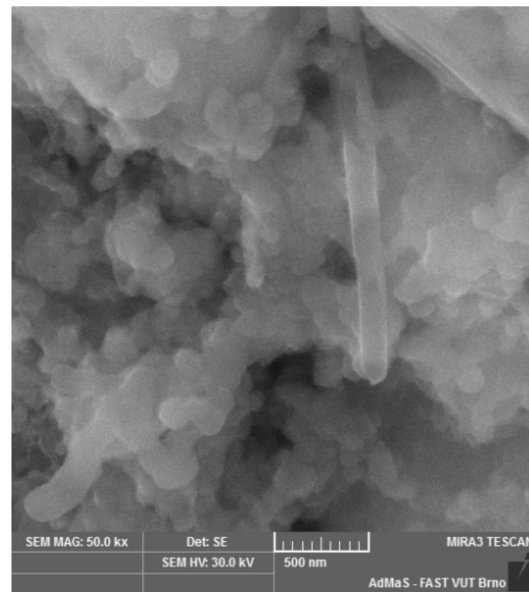


**Figure 3.** Morphology of cement hydration products with nanotubes at the induction period of hydration (about 1 hour after cement paste mixing).

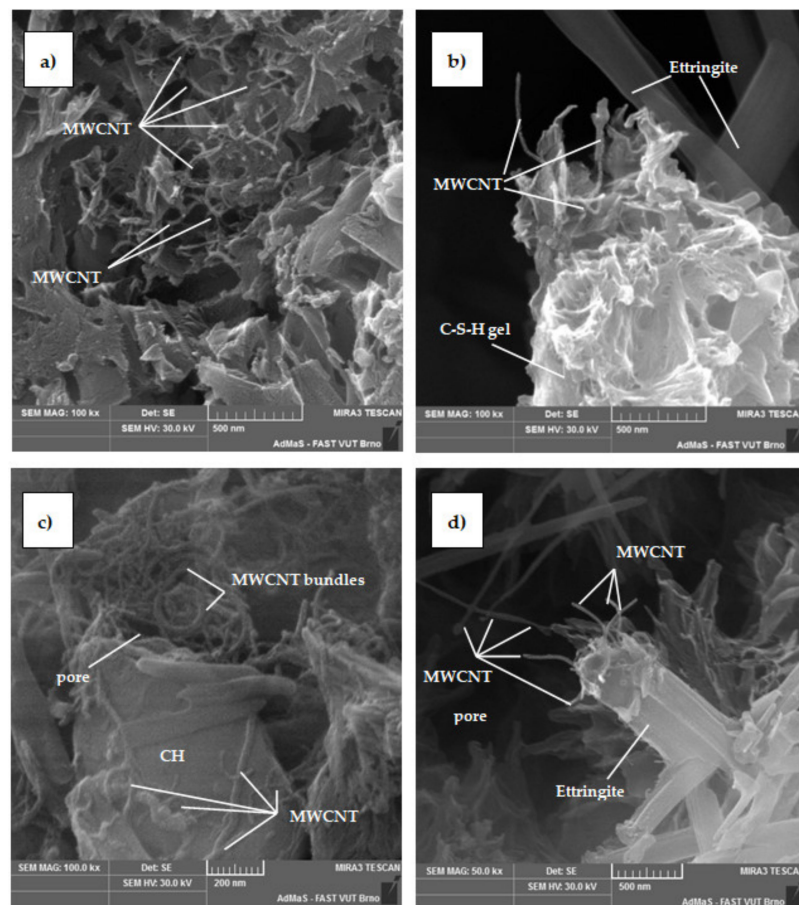


**Figure 4.** Morphology of cement hydration products with nanotubes at an age of 3 days: (a) general view of the distribution of nanotubes among cement hydration products; (b) overgrowth of nanotubes by C-S-H gel; (c) distribution of nanotubes on the surface of portlandite (CH) and filling of gel pores by nanotube bundles; (d) overgrowth of nanotubes on ettringite.

This observation can note the nucleation effect of nanotubes, which can improve the formation of cement hydration products such as sulfoaluminates, calcium hydrosilicates, etc. The nucleation effect of nanotubes in the cement matrix was highlighted in a number of previous studies [25,31]. Another part of MWCNTs is not covered by cement hydration products. This aspect can indicate the lack of chemical interactions between nanotubes and cement hydration products. The inert character of carbon-based materials without additional functionalization was also highlighted in previous research [12,42]. MWCNTs in the bottom-left corner of the SEM image have a curved shape, which can be caused by the high differences between the diameter of the nanotubes and their length. High-concentrated MWCNTs can be distributed in the unfilled porosity volumes in bent or twisted shapes. The reason for MWCNT bending or rotation can be a mechanical effect of concentrated MWCNT volume during high-speed cement paste mixing. This shape of nanotubes remains after the hardening processes of cement paste, and reduces the volume of capillary pores in hardened cement paste.

X-ray diffraction patterns of hardened cement paste with nanotubes in the dosages from 0 to 0.12% bwoc at 28 days of curing are presented in Figure 5. The XRD pattern of the reference sample indicates the formation of portlandite  $\text{Ca}(\text{OH})_2$  (d-spacing: 0.494, 0.310, 0.263, 0.193, 0.179, 0.168 nm), peaks of calcium carbonate  $\text{CaCO}_3$  (d-spacing: 0.302, 0.209 nm), and the presence of unhydrated  $\text{C}_3\text{S}$  (d-spacing: 0.295, 0.286, 0.272, 0.218, 0.176 nm) and  $\text{C}_2\text{S}$  (d-spacing: 0.295, 0.275, 0.272, 0.218, 0.176 nm). The addition of MWCNTs did not cause the formation of new phases that can highlight the lack of chemical interactions between nanotubes and cement hydrates.

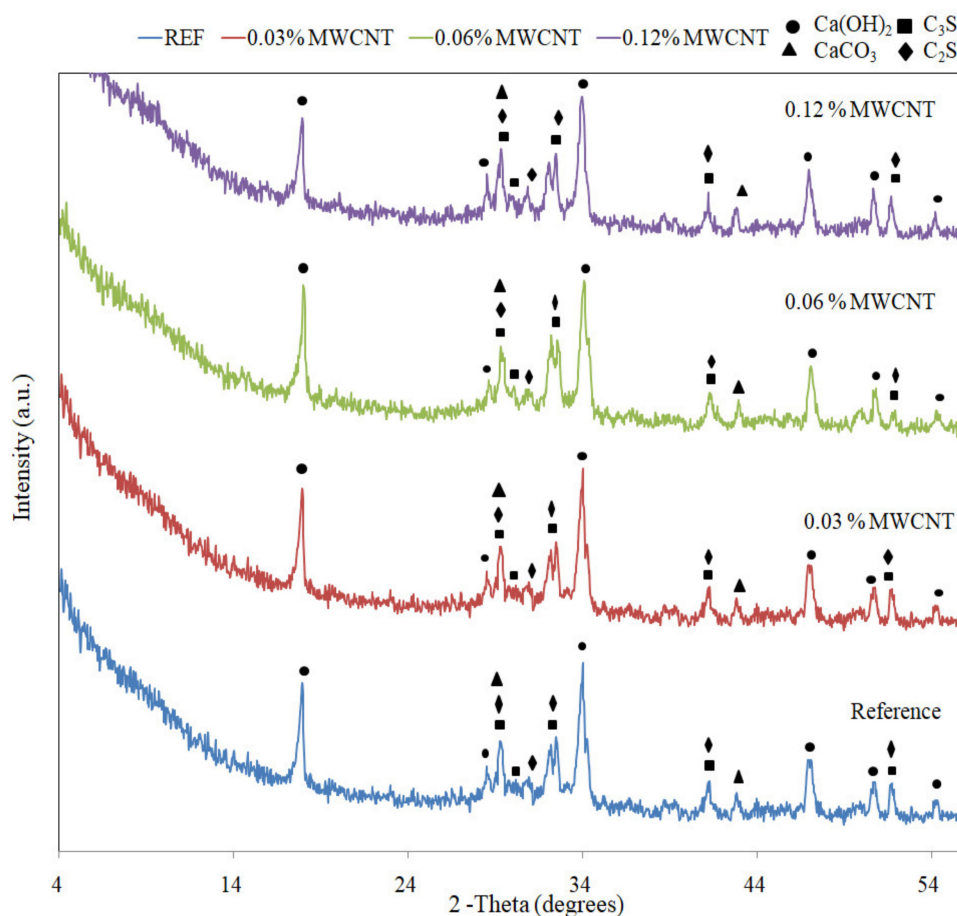


**Figure 5.** X-ray diffraction patterns of hardened cement paste with nanotubes cured for 28 days under normal conditions.

In all of the differential scanning calorimetry (DSC) patterns of hardened cement paste with nanotubes in dosages from 0 to 0.12% bwoc at 28 days of curing (Figure 6), endothermic effects at 100–200 °C (dehydration of cement hydration products), 430–450 °C (decomposition of portlandite), and 650–750 °C (decomposition of calcite) were established. The observed peaks for reference and modified samples have almost the same intensity, and occur at temperatures that do not vary remarkably.

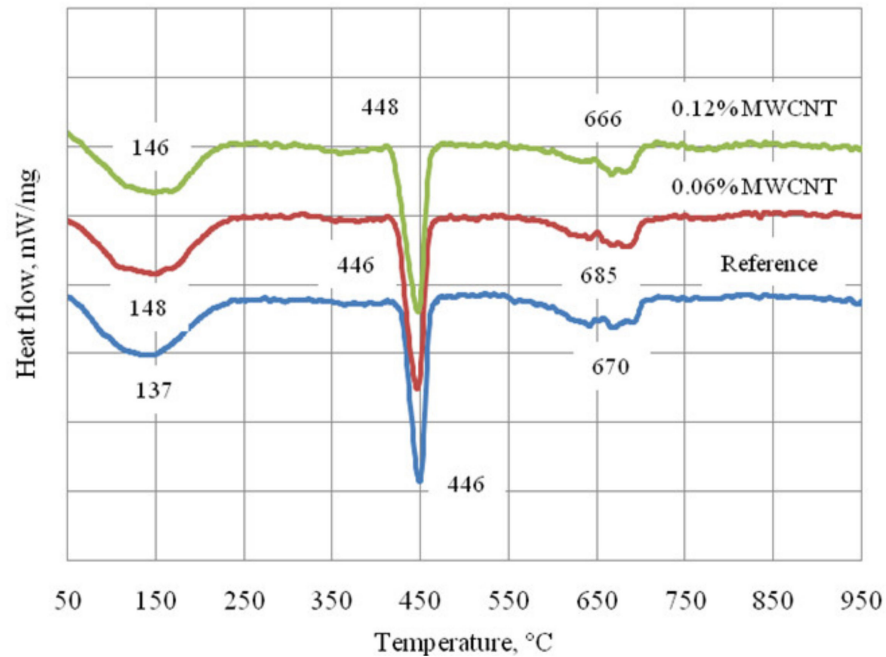


**Figure 6.** Differential scanning calorimetry patterns of samples with different amounts of the MWCNTs cured for 28 days under normal conditions.

The results of the thermogravimetric (TG) analysis are listed in Table 5. The mass loss related to dehydration of cement hydration products (~145 °C) decreased from 6.60 to 6.36 wt.% with an increase in nanotube dosage. The crucial point in the DSC curves is the decomposition of portlandite (~447 °C). The addition of nanotubes did not have a remarkable impact on the mass loss related to portlandite. The mass loss was 3.0 wt.% for reference sample without admixture, and 3.06 wt.% for the sample modified with 0.12% MWCNTs. Decomposition of calcite (~674 °C) was associated with the decrease in the mass loss from 1.69% to 1.40% with the increase in MWCNT dosage. The absence of any remarkable changes in the TG and DSC of nanomodified samples can also confirm the absence of any chemical interactions between nanotubes and cement hydration products.

**Table 5.** Results of thermogravimetric analysis.

Sample	90–200 °C	430–465 °C	650–750 °C
	Mass Loss, wt. %	Mass Loss, wt. %	Mass Loss, wt. %
Reference	6.60	3.00	1.69
0.06% MWCNT	6.43	3.05	1.52
0.12% MWCNT	6.36	3.06	1.40

The Fourier-transform infrared spectroscopy (FTIR) of hardened cement paste without nanotubes and with 0.12% bwoc is presented in Figure 7. The following peaks were established: symmetric and asymmetric O–H stretching ( $\nu_1$  and  $\nu_3$ ) of  $\text{Ca}(\text{OH})_2$  ( $3645\text{ cm}^{-1}$ ;  $3419\text{ cm}^{-1}$ ) [43,44]; deformation mode H–O–H ( $\nu_2$ ) ( $1650\text{ cm}^{-1}$ ) [44]; vibrations of carbonate,  $\text{CO}_3^{2-}$  ( $1435\text{ cm}^{-1}$ ,  $875\text{ cm}^{-1}$  and  $729\text{ cm}^{-1}$ ) [43–45]; vibration ( $\nu_3$ ) of the  $\text{SO}_4^{2-}$  group

in sulfates ( $1124\text{ cm}^{-1}$ ,  $1127\text{ cm}^{-1}$ ) [46]; stretching ( $\nu_3$ ) of Si–O ( $950\text{ cm}^{-1}$ ,  $975\text{ cm}^{-1}$ ) [44]; and bending vibration ( $\nu_4$  and  $\nu_2$ ) of  $\text{SiO}_4^{4-}$  ( $465\text{ cm}^{-1}$ ,  $524\text{ cm}^{-1}$ ) [43,47].

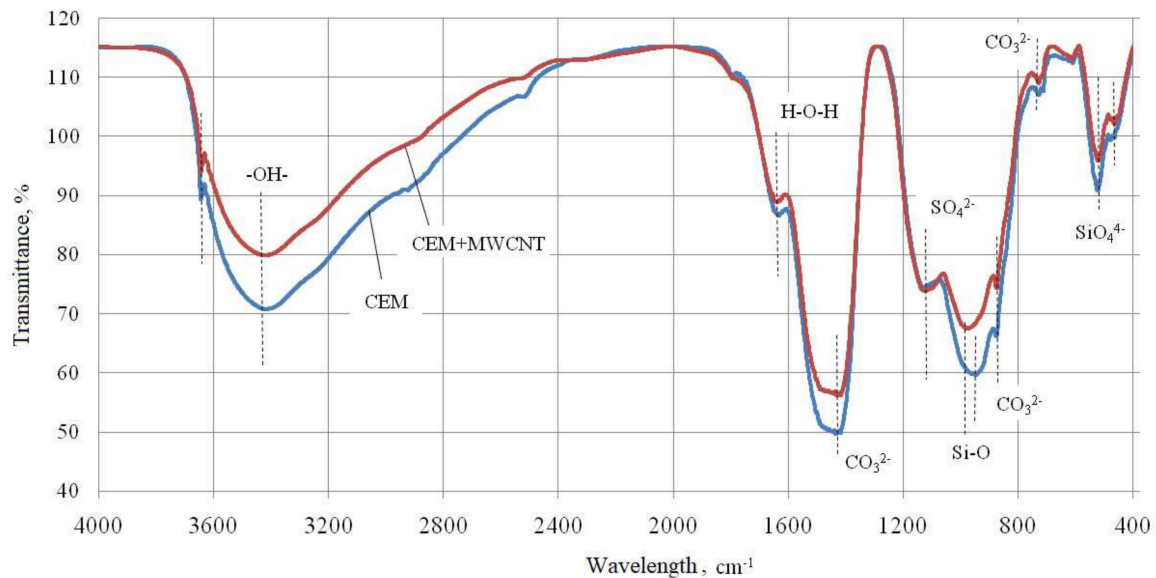


**Figure 7.** Fourier-transform infrared spectroscopy for the nanomodified hardened cement paste cured for 28 days under normal conditions.

FTIR spectroscopy did not reveal new chemical bonds, which can also confirm the absence of chemical interactions between MWCNTs and cement systems. However, some changes in the intensity of the peaks at  $3645\text{ cm}^{-1}$ ,  $3419\text{ cm}^{-1}$ , and  $1640\text{ cm}^{-1}$  can be associated with the retardation of the cement hydration with the formation of less  $\text{Ca}(\text{OH})_2$ . Such changes can be linked to the presence of CMC in the MWCNT suspension, and to the interactions between functional groups of CMC and  $\text{Ca}^{2+}$  ions of cement. Moreover, no remarkable changes should be noted for the peaks at  $975\text{ cm}^{-1}$ ,  $465\text{ cm}^{-1}$ , and  $524\text{ cm}^{-1}$ , which can be attributed to the changes in the formation of calcium hydrosilicates. MWCNTs do not cause any chemical interactions; however, the presence of CMC in the suspension can cause some changes during cement hydration.

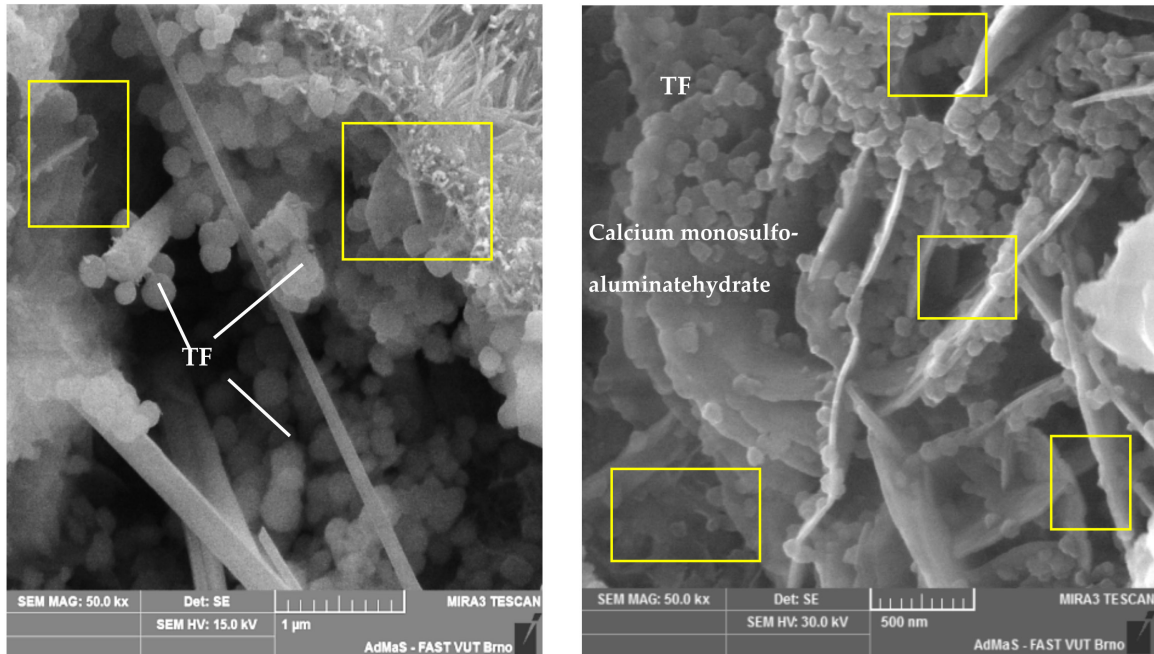
### 3.2. Carbon Black

The modification with CB paste can be similar to the modification with nanotubes, since the carbon surface of CB is also inert to the cement hydration products. CB is present in the mixing water before the cement hydration; therefore, cement hydrates can be formed on the surface of ultrafine particles of the additive.

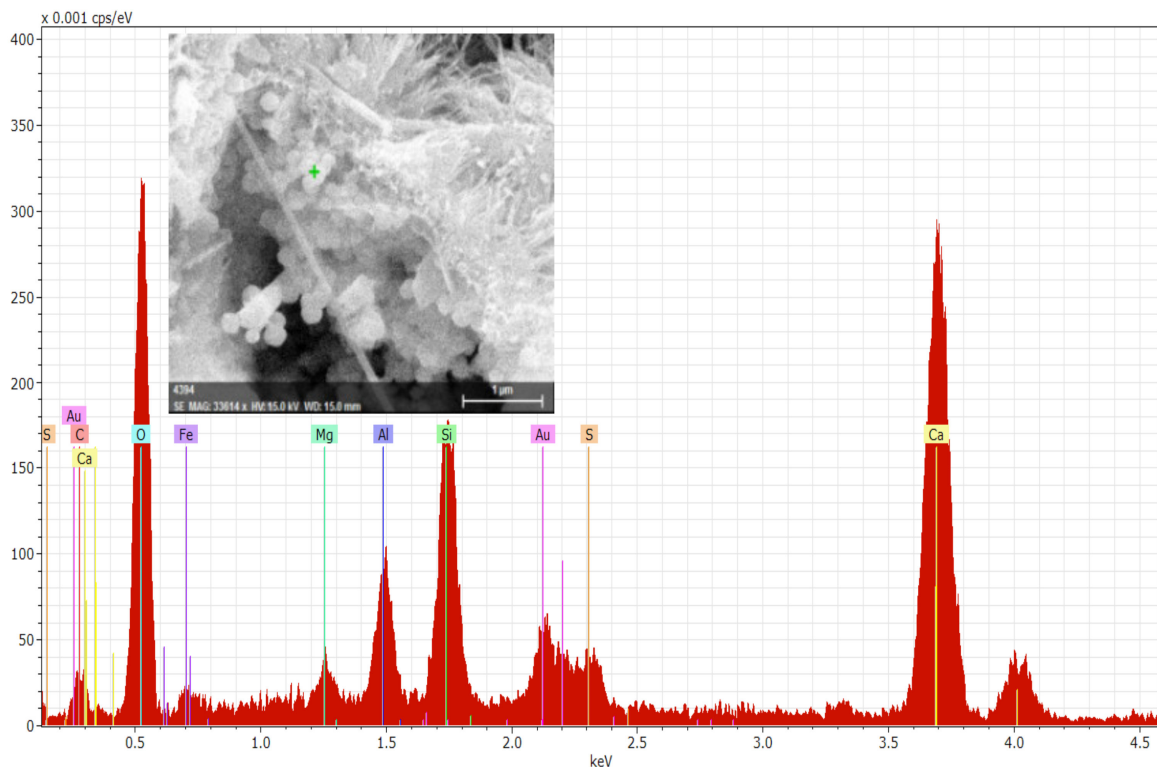
Figure 8 presents the SEM images of cement paste with CB at a dosage of 0.005% bwoc. SEM revealed ettringite, calcium monosulfoaluminate hydrate, fibers of C–S–H gel, and spherical formations with a size of  $\sim 100\text{ nm}$ . The spherical hydration products can be attributed to the thaumasite formations (TFs) ( $3\text{CaO}\cdot\text{SiO}_2\cdot\text{CO}_2\cdot\text{SO}_3$ ), which can be obtained through the reaction of calcium silicate hydrate (C–S–H) with calcite and unbound sulfate ions or, in case of the reaction between ettringite and C–S–H, with carbonates/bicarbonates [48–51]. In order to obtain the elemental analysis of the observed spherical hydration products, EDX analysis was performed (Figure 8b). The placement of CB among the cement hydration products is evidenced by the yellow frame in the SEM images in Figure 8a.

The carbon black particles are oriented near the cement hydration products—calcium silicate hydrate (C–S–H) microfibers, calcium monosulfoaluminate hydrates, and spherical thaumasite crystals. The thaumasite particles are more crystallized on the surfaces of monosulfoaluminate hydrates with thicker plates. Only a small quantity of spherical thaumasite crystals is oriented on the surface of flaky carbon black (CB) crystals with

thickness less than 80 nm. The empty surfaces of CB not covered by cement hydration products indicate the absence of strong adhesion with cement hydration products due to the low chemical reactivity of carbon. However, irregularly oriented CB crystals reduce the volume of capillary pores in hardened cement paste.



(a)



(b)

**Figure 8.** (a) Morphology of cement hydrates with carbon black at an age of 28 days. (b) Energy-dispersive spectroscopy analysis.

To investigate the composition of new cement hydration products, thermal analysis was performed (Figure 9).

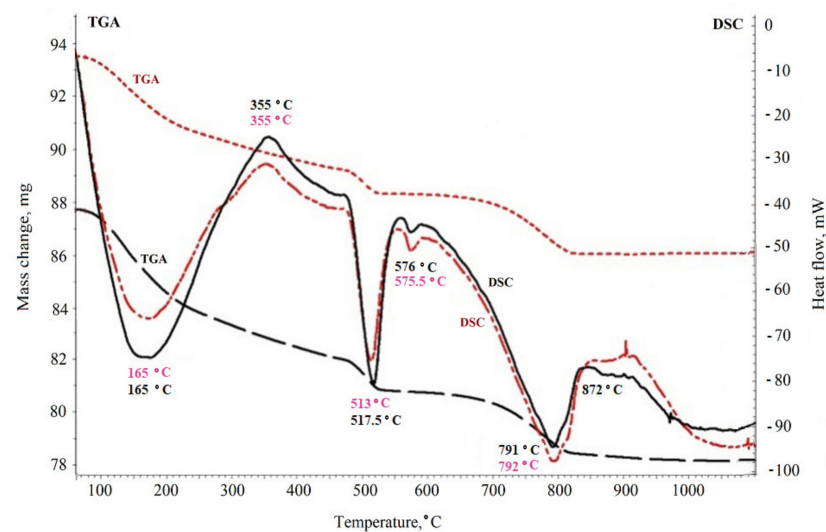


**Figure 9.** Differential scanning calorimetry and thermogravimetric analysis patterns of samples with carbon black cured for 28 days under normal conditions (black curves: sample without additives; red curves: sample modified with 0.005% carbon black).

DSC revealed the endothermic effects at 100–200 °C, 450–550 °C, and 700–800 °C. The exothermic effect with peaks at ~900 °C was attributed to the crystallization of calcium hydrosilicates. With the addition of CB, this exothermic effect was more intensive in comparison with the sample without additives. These differences can be linked to the basicity of the formed hydrosilicates in case of modification with CB paste.

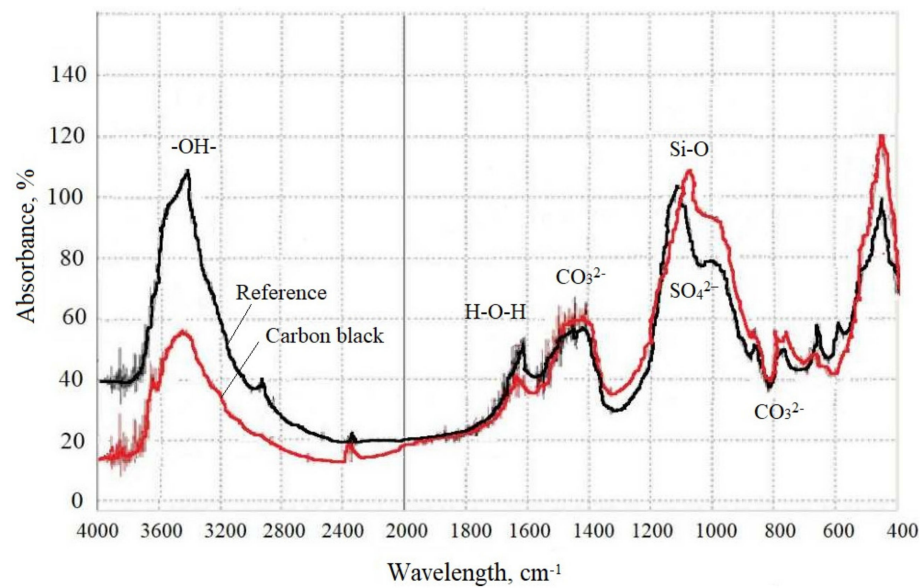
IR spectroscopy showed significant differences in the spectra for samples modified with CB in comparison with the reference sample (Figure 10). The decrease in the intensity of the absorption peak at  $1008.7\text{ cm}^{-1}$  and shift in the absorption peaks from  $1120.64\text{ cm}^{-1}$  to  $1087.85\text{ cm}^{-1}$  can be associated with  $\nu_3$  stretching of Si–O [44] and  $\nu_3$  vibration of the  $\text{SO}_4^{2-}$  [46], respectively. The observed effects highlight the differences in the formation of calcium hydrosilicates of cement paste modified with CB. Absorption peaks at  $3385.07\text{ cm}^{-1}$  and  $1637.58\text{ cm}^{-1}$  corresponding to O–H stretching ( $\nu_1$  and  $\nu_3$ ) of  $\text{Ca}(\text{OH})_2$  [43,44] and the deformation mode H–O–H ( $\nu_2$ ) [44] can confirm a slight decrease in the amount of free calcium hydroxide due to its binding to calcium hydrosilicates; this is consistent with results obtained by thermal analysis at a temperature of 513 °C.

Taking into account the results of SEM, thermal analysis, and IR spectroscopy, it is possible to conclude the intensification of the cement hydration process with the formation of low-base calcium hydrosilicates due to modification with CB.

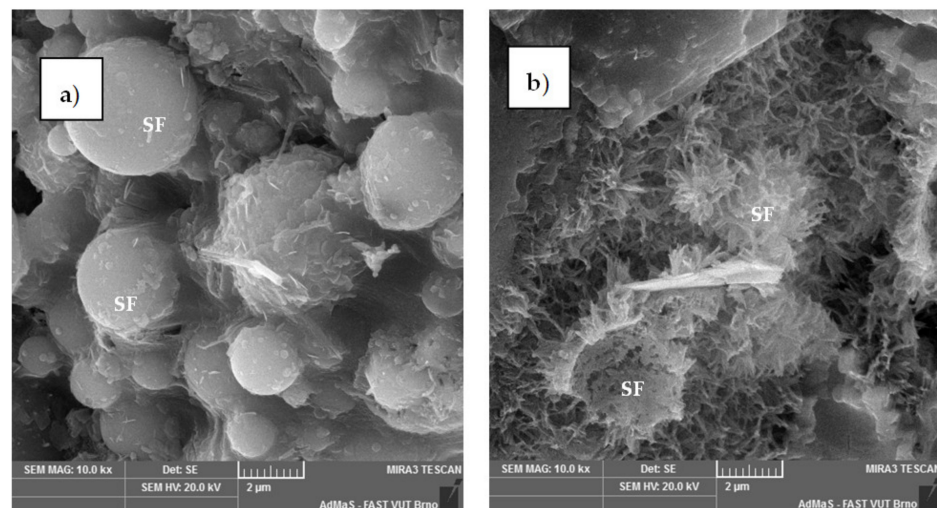
### 3.3. Silica Fume and Complex Modification with Silica Fume and Nanotubes

Figure 11 shows the morphology of cement hydration products in case of modification with SF. Due to the pozzolanic reaction, hydrosilicates with fiber-shaped forms can be crystallized on the surface of the fine spherical particles of SF.

Figure 11a shows the surface of SF covered with the cement hydration products at the beginning of the hydration process, whereas in Figure 11b it is possible to observe the more intensive formation of hydrosilicates around the SF's surface during hydration. Both pictures show high adhesion between SF and cement hydration products. The formation of denser microstructure with the addition of SF, as shown in Figure 11b, enables the obtainment of cement-based materials with higher density, strength characteristics, and durability [32–34].



**Figure 10.** Infrared spectroscopy for the hardened cement paste modified with carbon black paste cured for 28 days under normal conditions.



**Figure 11.** Morphology of cement hydration products modified by silica fume at age of 28 days.

The combined modification of cement paste with SF and inert carbon nanotubes can lead to the additional densification and reinforcement of the cement matrix (Figure 12). The SEM images presented in Figure 12 reveal the presence of ettringite and SF covered with the cement hydration products. Furthermore, the SEM image reveals the presence of nanotubes equally distributed among calcium silicate hydrate phases.

DSC analysis (Figure 13) for samples modified with SF and nanotubes revealed the typical endothermic effects for hardened cement paste (see description of DSC for previous samples). The more intensive decrease in the endothermic effects at  $\sim 500$  °C attributed to the decomposition of portlandite was observed for the modified sample in comparison with the reference sample. This effect can be associated with the linkage to portlandite by SF. The pozzolanic reaction between portlandite and silica fume causes the formation of hydrosilicates with different basicity. In addition to the thermal analysis, IR spectroscopy was undertaken for samples with SF and nanotubes (Figure 14).

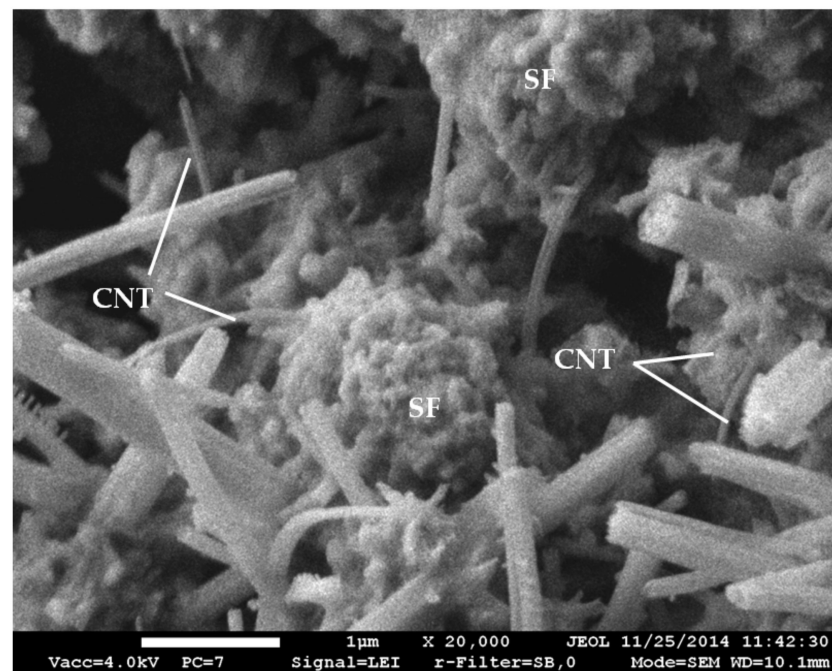


**Figure 12.** Morphology of cement hydration products modified with silica fume and nanotubes at an age of 28 days.

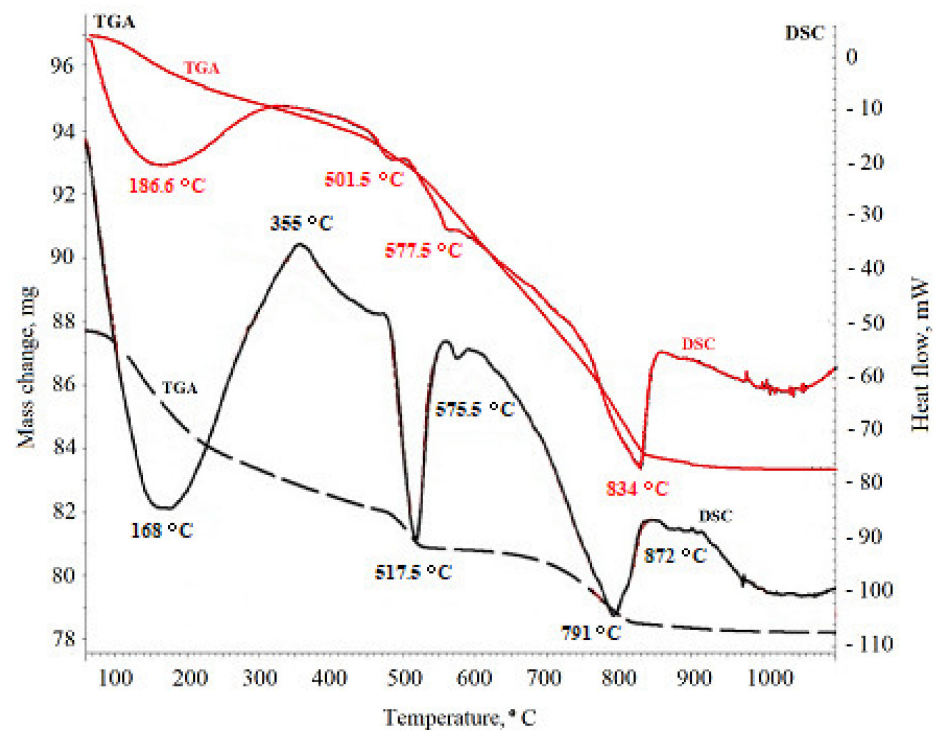


**Figure 13.** Differential scanning calorimetry and thermogravimetric analysis patterns of samples with silica fume and nanotubes cured for 28 days under normal conditions (black curves: sample without additives; red curves: sample modified with 0.005% MWCNTs and 3% SF).

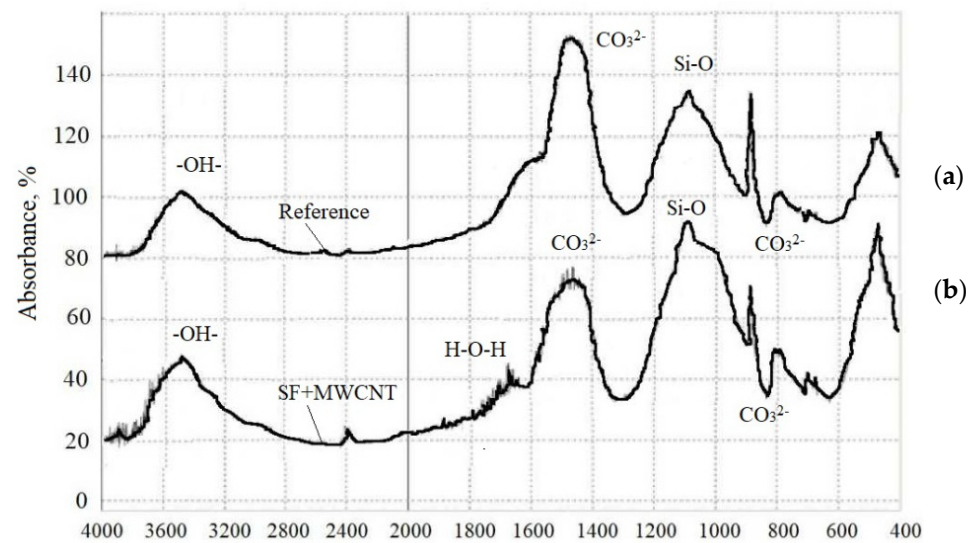


**Figure 14.** Infrared spectroscopy for the hardened cement paste modified with silica fume and nanotubes and cured for 28 days under normal conditions: (a) reference sample; (b) modified sample.

The modification with SF and MWCNTs leads to an increase in absorption peaks ( $1085$  and  $1033\text{ cm}^{-1}$ ) and the appearance of an additional absorption peak at  $1033\text{ cm}^{-1}$ , which can be attributed to Si–O stretching vibration [51]. The differences were also established for absorption peaks at  $3200\text{--}3600\text{ cm}^{-1}$  and  $1650\text{ cm}^{-1}$ , corresponding to O–H stretching of  $\text{Ca}(\text{OH})_2$  and deformation mode H–O–H ( $\nu_2$ ) of the molecular water absorbed, respectively [43,44]. The observed differences in adsorption lines in case of complex modification with SF and nanotubes can be a confirmation for the pozzolanic reaction between SF and portlandite, with a consequent formation of hydrosilicates with different basicity.

#### 4. Discussion

The main effect of modification in the case of the addition of ultrafine additives to the cement systems is provided by a directed effect on the processes of cement hydration, with subsequent crystallization of new formations with varying morphology. The introduction of ultrafine additives ensures the structuring of new formations with a change in their morphology, with the further formation of a modified cement matrix.

It is necessary to take into account the heterogeneity of the hardening cement matrix and the mutual influence of hydration products of Portland cement minerals on the mineralogical composition of new formations. At the same time, ultrafine additives with their low concentrations are not able to affect the mineralogy of the cement matrix. However, the high specific surface area of additives makes it possible for them to be a center of crystallization in supersaturated systems and form new polymorphic structures due to their geometric affinity for crystallizing formations [25,31].

As a result, the presence of ultrafine additives leads to changes in the morphology of cement hydration, the character of their intergrowth causing compaction of the structure of the hydrated cement matrix and improvements in the physical and mechanical properties of cement composites. The observed changes in the morphology of hardened cement paste in case of its modification with ultrafine additives of different origins are presented in Table 6.

The morphology of cement hydration products, such as calcium hydroxide and calcium silicate hydrates of different basicity, can be adjusted in the direction of the densification of the cement matrix structure in case of modification with ultrafine additives of different size and origins. The applied additives can be considered “preforms” [52], which provide accelerated crystallization of the supersaturated liquid phase in a hardening process of cement paste.

**Table 6.** Features of the morphology of hardened cement paste modified with ultrafine additives of different origin.

Type of Ultrafine Additive	Form and Size of the Additive	Applied Dosage of Additive, % bwoc	Observed Morphology of Cement Hydrates
Multi-walled carbon nanotubes	Filaments with a diameter of ~15–20 nm and length of 0.1–10 $\mu\text{m}$	0.25	Overgrowth of nanotubes by cement hydration products (C–S–H gel, portlandite, ettringite); filling pores with nanotube bundles; reinforcement of cement matrix; the surface of the tubes is uncovered by hydration products.
Carbon black	Nanoplates with size from 40 to 170 nm	0.005	Formation of ettringite, calcium monosulfate hydrate, fibers of calcium silicate hydrates, and thaumasite formations. Placement of carbon black inside the cement hydration products (such as calcium monosulfate hydrate or C–S–H gel).
Silica fume	Particles of spherical shape with a diameter of ~300 nm	3	Formation of C–S–H gel, portlandite, and ettringite. Silica fume is covered with calcium silicate hydrates and has strong adhesion with them.
Complex of silica fume and nanotubes	See parameters for silica fume and nanotubes above	0.005 (nanotubes) and 3 (silica fume)	Needles of ettringite; C–S–H gel. Silica fume covered with calcium silicate hydrates. Nanotubes growing from the cement hydration products, with the absence of their covering with the cement hydration products.

The morphology of the hydrates is determined by the degree of dispersion of the ultrafine additive, its origin, and its geometry (Table 6). The increase in the density of the final microstructure of the cement matrix is achieved not only by changing the final shape of the calcium silicate hydrates, but also by the densification of the contacts between separate hydrates.

Moreover, the interactions between the surfaces of additives and cement hydration products should be taken into consideration. In the case of carbon nanomaterials, such as nanotubes and carbon black, the inert nature of carbon does not lead to the formation of hydrates on its surface with strong adhesion between them (Figures 3, 4 and 8) [12,45]. In the case of ultrafine additives with amorphous  $\text{SiO}_2$ , a pozzolanic reaction takes place (Figure 11) [33,34]. Figure 15 shows the proposed explanation of the formation of the microstructure of hardened cement pastes modified with ultrafine additives.

In the case of the reference sample without additives, it is possible to observe the standard formation of C–S–H gel, portlandite, and ettringite during the cement hardening process (Figure 15a).

The addition of the MWCNT suspension as part of the mixing water, firstly, can affect changes in the electrokinetic properties of the water, with further changes in the crystallization process. Nanotubes are inert to cement hydration products; therefore, their mechanisms in the cement matrix can be caused only by physical effects. Figure 15b shows the possible distribution of nanotubes in the cement systems before and after the hydration process. The mechanism of action of CB in the cement systems is similar to the mechanism of MWCNTs. However, the different geometry of MWCNTs and CB can cause some contrast between the formed calcium silicate hydrates placed on the surface of the nanoadditives.

Modification of cement systems with SF is accompanied by a pozzolanic reaction with portlandite, which leads to the formation of calcium silicate hydrates with strong adhesion to the SF particles' surface (Figure 11). Figure 15c shows the hydration process in case of the addition of SF to the cement system. The mechanism of SF in cement systems can be explained not only by physical effects, but also by chemical interactions (pozzolanic reaction).

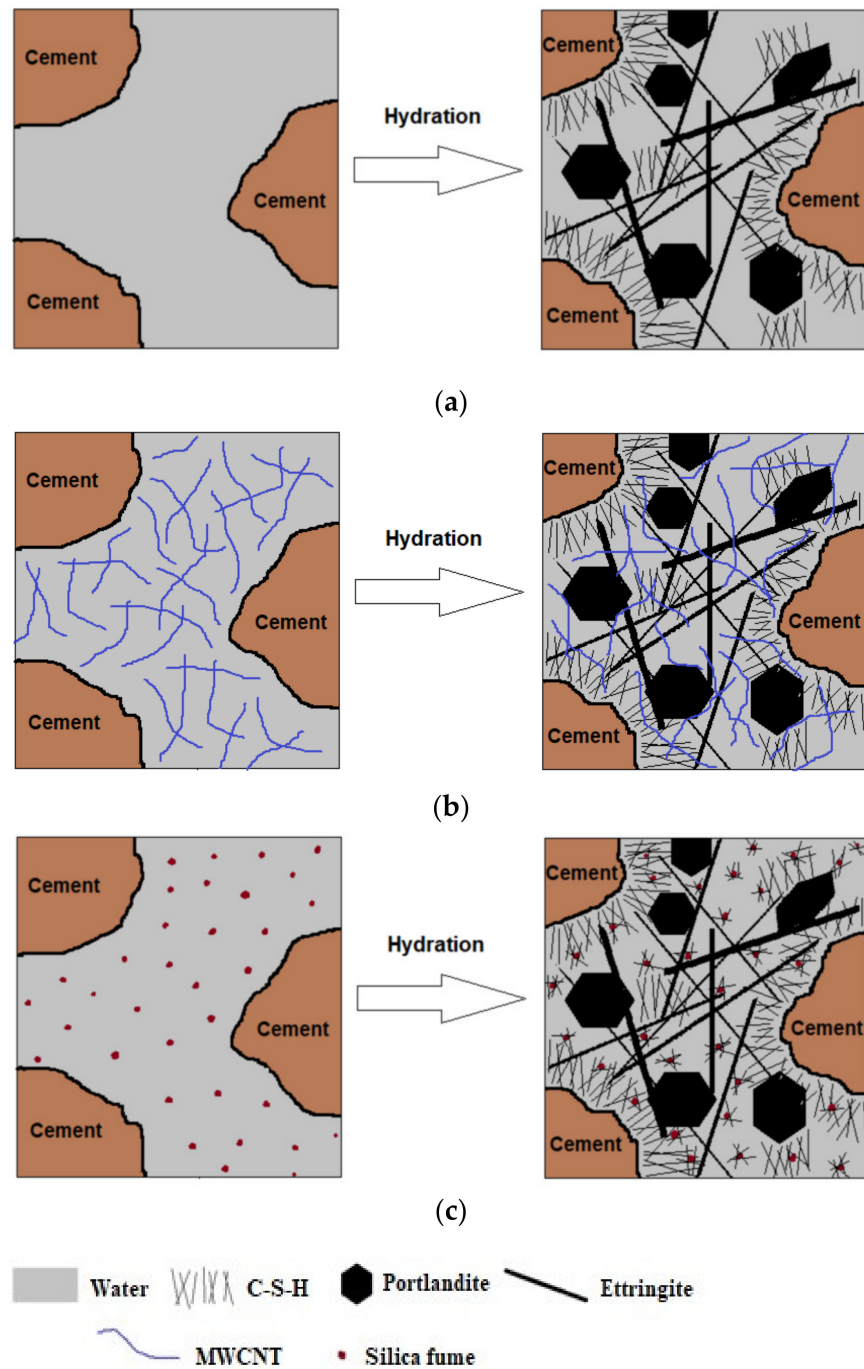


**Figure 15.** Scheme of the cement paste before and after hydration: (a) without additives; (b) with multi-walled carbon nanotubes (MWCNTs); (c) with silica fume.

## 5. Conclusions

The present research is focused on the investigation of hardened cement paste modified with ultrafine additives of different origins, which determine the morphological transformations and affect the properties of hydrated cement products. In the course of the research, the modification of ordinary Portland cement was performed via both non-reactive multi-walled carbon nanotubes (MWCNTs) and carbon black (CB) paste, and silica fume (SF) with high reactivity. The chemical activity, specific surface, and shape of the particles predetermine the morphological transformation and microstructure of hardened cement paste and, furthermore, the properties and durability of the hardened cement paste.

The following conclusions can be drawn based on the obtained results:

1. The usage of ultrafine additives of different sizes and origins allows management of the morphology of cement hydration products with the formation of energy-efficient, stable structures with increased nucleation rates and compactness, with a consequent improvement in the physical and mechanical characteristics of hardened cement paste;
2. The morphology of hardened cement paste depends on the chemical activity of the additives. Modification with the inert additives (carbon black, nanotubes) leads to the formation of the cement hydration products on their surface without strong adhesion, whereas chemically active additives (silica fume) possess high adhesion to cement hydration products;
3. In the case of the usage of the active ultrafine additive (silica fume), its pozzolanic reaction with calcium hydroxide contributes to the formation of additional content of calcium silicate hydrates, with strong adhesion to the surface of silica fume particles. The improvement of the microstructure of cement matrix through the addition of silica fume enables the reduction of the porosity of hardened cement paste, and increases the mechanical properties and durability of hardened cement paste;
4. The microstructure of hardened cement paste depends on the geometry of the ultrafine additive. Filaments of nanotubes are distributed between calcium silicate hydrates, and can work as reinforcement and nucleation centers. In the case of the usage of carbon black with flat surfaces, the carbon black crystals are oriented in empty volumes with low adhesion to cement hydration products due to the low chemical reactivity of carbon. The spherical particles of silica fume are fully and equally covered by the cement hydration products in the hydration processes due to the pozzolanic reaction;
5. The comparison between different ultrafine additives and the complex additives based on them can lead to the obtainment of effective additives with suitable prices for construction practice.

Despite the significant number of studies on this topic, the effects of ultrafine additives and different complex additives based on them should be investigated further. Such factors as the shape and size of particles, chemical reactivity to cement hydration products, and the type and intensity of their homogenization in water and cement-based composites are important for the evaluation of complex additives for high-performance concrete mixtures. Moreover, the high cost of nanoadditives requires searching for reasonable ways to investigate ultrafine additives based on industrial waste that can work as effective additives for concrete modification.

**Author Contributions:** Conceptualization, G.Y., G.S., L.U. and R.D.; methodology, I.P. (Irina Polyanskikh), I.P. (Igor Pudov) and E.K.; software, I.P. (Irina Polyanskikh), I.P. (Igor Pudov) and E.K.; validation, G.Y., G.S., L.U. and R.D.; formal analysis, I.P. (Irina Polyanskikh); investigation, I.P. (Irina Polyanskikh), I.P. (Igor Pudov) and E.K.; resources, I.P. (Irina Polyanskikh), I.P. (Igor Pudov), E.K., Z.S. and A.E.M.M.E.; data curation, G.Y., G.S. and R.D.; writing—original draft preparation, G.Y., G.S., E.K. and Z.S.; writing—review and editing, I.P. (Irina Polyanskikh) and G.Y.; visualization, I.P. (Igor Pudov), Z.S. and A.E.M.M.E.; supervision, G.Y.; project administration, G.Y., L.U. and R.D. All authors have read and agreed to the published version of the manuscript.

**Funding:** The reported study was funded by the Russian Foundation for Basic Research and the Czech Science Foundation according to the research project № 19-53-26011.

**Data Availability Statement:** The data presented in this study are available on request from the corresponding author.

**Acknowledgments:** We are grateful to the Russian Foundation for Basic Research and the Czech Science Foundation for funding the research project.

**Conflicts of Interest:** The authors declare no conflict of interest.

## References

1. Sun, J.; Zhan, Z.; Hou, G. Utilization of fly ash microsphere powder as a mineral admixture of cement: Effects on early hydration and microstructure at different curing temperatures. *Powder Technol.* **2020**, *375*, 262–270. [[CrossRef](#)]
2. Ilic, B.L.; Radonjanin, V.; Malesev, M.; Zdujic, M.; Mitrovic, A. Study on the addition effect of metakaolin and mechanically activated kaolin on cement strength and microstructure under different curing conditions. *Constr. Build. Mater.* **2017**, *133*, 243–252. [[CrossRef](#)]
3. Liu, J.; Fu, J.; Yang, Y.; Gu, C. Study on dispersion, mechanical and microstructure properties of cement paste incorporating graphene sheets. *Constr. Build. Mater.* **2017**, *199*, 1–11. [[CrossRef](#)]
4. MacLeod, A.J.N.; Collins, F.G.; Duan, W.; Gates, W.P. Quantitative microstructural characterisation of Portland cement-carbon nanotube composites using electron and x-ray microscopy. *Cem. Concr. Res.* **2019**, *123*, 105767. [[CrossRef](#)]
5. Tan, Y.; Yu, H.; Sun, S.; Wu, C.; Ding, H. Properties and microstructure of basic magnesium sulfate cement: Influence of silica fume. *Constr. Build. Mater.* **2021**, *266*, 121076. [[CrossRef](#)] [[PubMed](#)]
6. Zhao, D.; Khoshnazar, R. Microstructure of cement paste incorporating high volume of low-grade metakaolin. *Cem. Concr. Compos.* **2020**, *106*, 103453. [[CrossRef](#)]
7. Ng, D.S.; Paul, S.C.; Anggraini, V.; Kong, S.Y.; Qureshi, T.S.; Rodriguez, C.R.; Liu, Q.; Savija, B. Influence of SiO<sub>2</sub>, TiO<sub>2</sub> and Fe<sub>2</sub>O<sub>3</sub> nanoparticles on the properties of fly ash blended cement mortars. *Constr. Build. Mater.* **2020**, *258*, 119627. [[CrossRef](#)]
8. Chen, J.; Akono, A.-T. Influence of multi-walled carbon nanotubes on the hydration products of ordinary Portland cement paste. *Cem. Concr. Res.* **2020**, *137*, 106197. [[CrossRef](#)]
9. Korpa, A.; Kowald, T.; Trettin, R. Hydration behaviour, structure and morphology of hydration phases in advanced cement-based systems containing micro and nanoscale pozzolanic additives. *Cem. Concr. Res.* **2008**, *38*, 955–962. [[CrossRef](#)]
10. Mehairi, A.G.; Husein, M.M. Enhancement of cement properties by means of in situ grown nanoparticles. *Constr. Build. Mater.* **2020**, *261*, 120496. [[CrossRef](#)]
11. Qi, X.; Zhang, S.; Wang, T.; Guo, S.; Ren, R. Effect of High-Dispersible Graphene on the Strength and Durability of Cement Mortars. *Materials* **2021**, *14*, 915. [[CrossRef](#)]
12. Li, Y.; Li, H.; Wang, Z.; Jin, C. Effect and mechanism analysis of functionalized multi-walled carbon nanotubes (MWCNTs) on C–S–H gel. *Cem. Concr. Res.* **2020**, *128*, 105955. [[CrossRef](#)]
13. Wang, L.; Zhang, S.; Zheng, D.; Yang, H.; Cui, H.; Tang, W.; Li, D. Effect of Graphene Oxide (GO) on the Morphology and Microstructure of Cement Hydration Products. *Nanomaterials* **2017**, *7*, 429. [[CrossRef](#)] [[PubMed](#)]
14. Monteiro, A.O.; Cachim, P.B.; Costa, P.M.F.J. Electrical properties of cement-based composites containing carbon black particles. *Mater. Today Proc.* **2015**, *2*, 193–199. [[CrossRef](#)]
15. Nalon, G.H.; Ribeiro, J.C.L.; Araujo, E.N.D.; Pedroti, L.G.; Carvalho, J.M.F.; Santos, R.F.; Aparecido-Ferreira, A. Effects of different kinds of carbon black nanoparticles on the piezoresistive and mechanical properties of cement-based composites. *J. Build. Eng.* **2020**, *32*, 101724. [[CrossRef](#)]
16. Dong, W.; Li, W.; Shen, L.; Sheng, D. Piezoresistive behaviours of carbon black cement-based sensors with layer-distributed conductive rubber fibres. *Mater. Design.* **2019**, *182*, 108012. [[CrossRef](#)]
17. Yakovlev, G.I.; Grahov, V.P.; Gordina, A.F.; Shaibadullina, A.V.; Saidova, Z.S.; Nikitina, S.V.; Begunova, E.V.; Elrefai, A.E.M.M. Influence of carbon black dispersion on the properties of fine-grained concrete. *Build. Mater.* **2018**, *8*, 89–92. [[CrossRef](#)]
18. Medina, N.F.; Barbero-Barrera, M.M.; Bustamante, R. Improvement of the properties of gypsum-based composites with recycled isostatic graphite powder from the milling production of molds for Electrical Discharge Machining (EDM) used as a new filler. *Constr. Build. Mater.* **2016**, *107*, 17–27. [[CrossRef](#)]
19. Grahov, V.; Mikhailov, Y.; Drochytka, R.; Kizinievich, O.; Ginchitskaya, Y.; Gordina, A. Structural ceramics modified with technogenic isostatic nanographite. *IOP Conf. Ser. Mater. Sci. Eng.* **2019**, *603*, 032070. [[CrossRef](#)]
20. Medina, N.F.; Barbero-Barrera, M.M.; Jove-Sandoval, F. Improvement of the mechanical and physical properties of cement paste sand mortars through the addition of isostatic graphite. *Constr. Build. Mater.* **2018**, *189*, 898–905. [[CrossRef](#)]
21. Xu, G.; Du, S.; He, J.; Shi, X. The role of admixed graphene oxide in a cement hydration system. *Carbon* **2019**, *148*, 141–150. [[CrossRef](#)]
22. Lv, S.; Liu, J.; Sun, T.; Ma, Y.; Zhou, Q. Effect of GO nanosheets on shapes of cement hydration crystals and their formation process. *Constr. Build. Mater.* **2014**, *64*, 231–239. [[CrossRef](#)]
23. Du, H.; Pang, S.D. Dispersion and stability of graphene nanoplatelet in water and its influence on cement composites. *Constr. Build. Mater.* **2018**, *167*, 403–413. [[CrossRef](#)]
24. Wang, B.; Pang, B. Mechanical property and toughening mechanism of water reducing agents modified graphene nanoplates reinforced cement composites. *Constr. Build. Mater.* **2019**, *226*, 699–711. [[CrossRef](#)]
25. Tafesse, M.; Kim, H.-K. The role of carbon nanotube on hydration kinetics and shrinkage of cement composite. *Compos. Part B* **2019**, *169*, 55–64. [[CrossRef](#)]
26. Echeverry-Cardona, L.M.; Alzate, N.; Restrepo-Parra, E.; Ospina, R.; Quintero-Orozco, J.H. Time-Stability Dispersion of MWCNTs for the Improvement of Mechanical Properties of Portland Cement Specimens. *Materials* **2020**, *13*, 4149. [[CrossRef](#)] [[PubMed](#)]
27. Arrechea, S.; Guerrero-Gutierrez, E.M.A.; Velasquez, L.; Cardona, J.; Posadas, R.; Callejas, K.; Torres, S.; Diaz, R.; Barrientos, C.; Garcia, E. Effect of additions of multiwall carbon nanotubes (MWCNT, MWCNT-COOH and MWCNT-Thiazol) in mechanical compression properties of a cement-based material. *Materialia* **2020**, *11*, 100739. [[CrossRef](#)]

28. Pan, J.; Cai, J.; Ma, H.; Leung, C.K.Y. Development of multiscale fiber-reinforced engineered cementitious composites with PVA fiber and CaCO<sub>3</sub> whisker. *J. Mat. Civil Eng.* **2018**, *30*, 04018106. [[CrossRef](#)]
29. Haghgoo, M.; Ansari, R.; Hassanzadeh-Aghdam, M.K.; Nankali, M. Analytical formulation for electrical conductivity and percolation threshold of epoxy multiscale nanocomposites reinforced with chopped carbon fibers and wavy carbon nanotubes considering tunnel ingrestitutivity. *Compos. Part A Appl. Sci. Manufact.* **2019**, *126*, 105616. [[CrossRef](#)]
30. Paul, S.C.; Rooyen, A.S.; Zijl, G.P.A.G.; Petrik, L.F. Properties of cement-based composites using nanoparticles: A comprehensive review. *Constr. Build. Mater.* **2018**, *189*, 1019–1034. [[CrossRef](#)]
31. Reales, O.A.M.; Filho, R.D.T. A review on the chemical, mechanical and microstructural characterization of carbon nanotubes-cement based composites. *Constr. Build. Mater.* **2017**, *154*, 697–710. [[CrossRef](#)]
32. Siddique, R. Utilization of silica fume in concrete: Review of hardened properties. *Resour. Conserv. Recycl.* **2011**, *55*, 923–932. [[CrossRef](#)]
33. Xu, W.; Zhang, Y.; Liu, B. Influence of silica fume and low curing temperature on mechanical property of cemented paste backfill. *Constr. Build. Mater.* **2020**, *254*, 119305. [[CrossRef](#)]
34. Jeong, Y.; Kang, S.-H.; Kim, M.O.; Moon, J. Acceleration of cement hydration from supplementary cementitious materials: Performance comparison between silica fume and hydrophobic silica. *Cem. Concr. Compos.* **2020**, *112*, 103688. [[CrossRef](#)]
35. Termkhajornkit, P.; Vu, Q.H.; Barbarulo, R.; Daronnat, S.; Chanvillard, G. Dependence of compressive strength on phase assemblage in cement pastes: Beyond gel-spaceratio—Experimental evidence and micromechanical modeling. *Cem. Concr. Res.* **2014**, *56*, 1–11. [[CrossRef](#)]
36. Krishnya, S.; Yoda, Y.; Elakneswaran, Y. A two-stage model for the prediction of mechanical properties of cement paste. *Cem. Concr. Compos.* **2021**, *115*, 103853. [[CrossRef](#)]
37. Wang, Q.; Li, S.; Pan, S.; Cui, X.; Corr, D.J.; Shah, S.P. Effect of graphene oxide on the hydration and microstructure of fly ash-cement system. *Constr. Build. Mater.* **2019**, *198*, 106–119. [[CrossRef](#)]
38. Wang, J.; Liu, M.; Wang, Y.; Zhou, Z.; Xu, D.; Du, P.; Cheng, X. Synergistic effects of nano-silica and fly ash on properties of cement-based composites. *Constr. Build. Mater.* **2020**, *262*, 120737. [[CrossRef](#)]
39. Song, C.; Hong, G.; Choi, S. Effect of dispersibility of carbon nanotubes by silica fume on material properties of cement mortars: Hydration, pore structure, mechanical properties, self-desiccation, and autogenous shrinkage. *Constr. Build. Mater.* **2020**, *265*, 120318. [[CrossRef](#)]
40. Skripkiunas, G.; Karpova, E.; Bendoraitiene, J.; Barauskas, I. Effect of MWCNT and PCE plasticizer on the properties of cement pastes. *IOP Conf. Ser. Mat. Sci. Eng.* **2019**, *660*, 012032. [[CrossRef](#)]
41. Khroustalev, B.M.; Leonovich, S.N.; Yakovlev, G.I.; Polyanskikh, I.S.; Lahayne, O.; Eberhardsteiner, J.; Skripkiunas, G.; Pudov, I.; Karpova, E.A. Structural modification of new formations in cement matrix using carbon nanotube dispersions and nanosilica. *Sci. Tech.* **2017**, *16*, 93–103. [[CrossRef](#)]
42. Sobolkina, A.; Mechtcherine, V.; Bergold, S.T.; Neubauer, J.; Bellmann, C.; Khavrus, V.; Oswald, S.; Leonhardt, A.; Reschetilowski, W. Effect of carbon-based materials on the early hydration of tricalcium silicate. *J. Am. Ceram. Soc.* **2016**, *99*, 2181–2196. [[CrossRef](#)]
43. Shi, T.; Gao, Y.; Corr, D.J.; Shah, S.P. FTIR study on early-age hydration of carbon nanotubes-modified cement-based materials. *Adv. Cem. Res.* **2019**, *31*, 353–361. [[CrossRef](#)]
44. Trezza, M.A. Hydration study of ordinary portland cement in the presence of zinc ions. *Mat. Res.* **2007**, *10*, 331–334. [[CrossRef](#)]
45. Parveen, S.; Rana, S.; Fanqueiro, R.; Paiva, M.C. Microstructure and mechanical properties of carbon nanotube reinforced cementitious composites developed using a novel dispersion technique. *Cem. Concr. Res.* **2015**, *73*, 215–227. [[CrossRef](#)]
46. Yang, H.; Monasterio, M.; Cui, H.; Han, N. Experimental study of the effects of graphene oxide on microstructure and properties of cement paste composite. *Compos. Part A* **2017**, *102*, 263–272. [[CrossRef](#)]
47. Souza, T.C.; Pinto, G.; Cruz, V.S.; Moura, M.; Ladeira, L.O. Evaluation of the rheological behavior, hydration process, and mechanical strength of Portland cement pastes produced with carbon nanotubes synthesized directly on clinker. *Constr. Build. Mater.* **2020**, *248*, 118686. [[CrossRef](#)]
48. Alksnis, F.F. *Hardening and Destruction of Gypsum-Cement Composite Materials*; Stroyizdat: Leningrad, Russia, 1988; p. 103. (In Russian)
49. Rahman, M.M.; Basuoni, M.T. Thaumassite sulfate attack on concrete: Mechanisms, influential factors and mitigation. *Constr. Build. Mater.* **2014**, *73*, 652–662. [[CrossRef](#)]
50. Mulenga, D.M.; Stark, J.; Nobst, P. Thaumassite formation in concrete and mortars containing fly ash. *Cem. Concr. Compos.* **2003**, *25*, 907–912. [[CrossRef](#)]
51. Accardo, G.; Cioffi, R.; Colangelo, F.; d’Angelo, R.; Stefano, L.; Paglietti, F. Diffuse reflectance Infrared Fourier Transform spectroscopy for the determination of asbestos species in bulk building materials. *Materials* **2014**, *7*, 457–470. [[CrossRef](#)]
52. Das, S.; Ray, S.; Sakar, S. Early strength development in concrete using preformed CSH nanocrystals. *Constr. Build. Mater.* **2020**, *233*, 117214. [[CrossRef](#)]